PHOTONICS Research

# Ultrafast optical nonlinearity of blue-emitting perovskite nanocrystals

Junzi Li,[1,†] Can Ren,[1,†] Xin Qiu,[1] Xiaodong Lin,[1] Rui Chen,[2] Cheng Yin,[3] and Tingchao He[1,*]

[1]College of Physics and Energy, Shenzhen University, Shenzhen 518060, China
[2]Department of Electrical and Electronic Engineering, South University of Science and Technology of China, Shenzhen 518055, China
[3]Department of Physics and Astronomy, Shanghai Jiao Tong University, Shanghai 200240, China
*Corresponding author: tche@szu.edu.cn

Received 10 January 2018; revised 18 March 2018; accepted 28 March 2018; posted 28 March 2018 (Doc. ID 318626); published 15 May 2018

**Perovskite nanocrystals (NCs) have strong nonlinear optical responses with a number of potential applications, ranging from upconverted blue-lasing to the tagging of specific cellular components in multicolor fluorescence microscopy. Here, we determine the one-photon linear absorption cross section of two kinds of blue-emitting perovskite NCs, i.e., $CsPbCl_3$ and $CsPb(Cl_{0.53}Br_{0.47})_3$, by utilizing femtosecond transient absorption spectroscopy. The wavelength-dependent nonlinear refraction and two-photon absorption have been measured at wavelengths from 620 to 720 nm by performing Z-scan measurements. The nonlinear optical responses of $CsPb(Cl_{0.53}Br_{0.47})_3$ are much more pronounced than those of $CsPbCl_3$ due to the larger structural destabilization of the former.** 

***OCIS codes:*** (190.7110) Ultrafast nonlinear optics; (320.7150) Ultrafast spectroscopy.

https://doi.org/10.1364/PRJ.6.000554

## 1. INTRODUCTION

The design, synthesis, characterization, and theoretical study of novel materials with nonlinear optical (NLO) responses [1,2] have been prompted by applications including optical limiting (OL), mode locking, bioimaging, and lasing [3–6].

Violet- and blue-emitting fluorescent NLO materials are particularly useful for these applications and others [7,8]. Although many design strategies have been developed that can efficiently enlarge NLO responses of materials with green to near-infrared light emission, studies of NLO materials with violet-blue emission properties are scarce [9–11].

Perovskite nanocrystals (NCs) that demonstrate superior optoelectronic properties for photovoltaics and light emission have recently demonstrated promising NLO properties, such as second-harmonic generation, multiphoton absorption (MPA), and MPA-pumped amplified lasing [12–17]. However, detailed understanding of the NLO properties of such perovskite NCs is still severely lacking; for example, the broad spectral dependence of their MPA cross sections and nonlinear refraction. Herein, by using femtosecond-transient absorption (fs-TA) spectroscopy, we have determined the one-photon linear absorption (OPLA) cross sections ($\sigma_{lin}$) of two kinds of blue-emitting perovskite NCs, i.e., $CsPbCl_3$ ($\sigma_{lin} \sim 4.3 \times 10^{-14}$ cm$^2$) and $CsPb(Cl_{0.53}Br_{0.47})_3$ ($\sigma_{lin} \sim 4.6 \times 10^{-14}$ cm$^2$). Furthermore, strong dependence of two-photon absorption (TPA) and nonlinear refraction on $CsPbCl_3$ and $CsPb(Cl_{0.53}Br_{0.47})_3$ NCs has been demonstrated for the first time. Experimental results show that the $CsPb(Cl_{0.53}Br_{0.47})_3$ NCs exhibit much higher TPA and intrinsic nonlinear refraction compared to $CsPbCl_3$ NCs.

## 2. EXPERIMENT

The $CsPbX_3$ NCs investigated here were synthesized following a recipe reported by Zeng *et al.* with slight modification. The detailed fabrication process can be found in Ref. [18].

The fluorescence quantum yields (QYs, $\eta$) of $CsPbCl_3$ and $CsPb(Cl_{0.53}Br_{0.47})_3$ NCs were, respectively, determined to be 6.9% and 13.1% using quinine sulfate monohydrate ($\eta_{350\,nm} = 0.58$) as a standard. The size and shape of the NCs were obtained by transmission electron microscopy (TEM) (JEOL, JEM-2010). Ultraviolet-visible (UV-Vis) absorption spectra of the samples were measured using a UV/Vis spectrometer (Lambda 950, PerkinElmer, Inc.) while the fluorescence and excitation spectra were measured using a fluorescence spectrophotometer (SENS-9000, Zolix). The values of the lifetime were determined using a compact luminescence lifeline spectrometer (C11367, Hamamatsu) with a C11367-11 photomultiplier tube. An light-emitting diode (LED) light source (365 nm, 1 MHz repetition rate) was used as the excitation source.

In the fs-TA experiments, the samples were pumped at 350 nm and probed with a white-light continuum. The probe pulses (350–750 nm) were generated by focusing a small portion (~1.5 μJ) of the fundamental 800 nm laser pulses on a thin $CaF_2$ plate. The linear polarization of the pump pulse

was adjusted to be perpendicular to that of the probe pulse with a polarizer and a half-wave plate. The cross-polarization is intended to eliminate any contribution from coherent artifacts. Pump-induced changes of transmission ($\Delta T/T$) of the probe beam were monitored using a monochromator/photomultiplier configuration with lock-in detection. The pump beam was chopped at 100 Hz, and this was used as the reference frequency for the lock-in amplifier.

The nonlinear refraction and TPA cross-sections of the NCs were measured using the closed- and open-aperture (CA and OA) Z-scan technique [19]. In the Z-scan measurements, the laser beam was focused onto the 1-mm-thick quartz cuvette filled with a solution of NCs by a spherical lens (focus length ~30 cm) and detected by a Si-based detector. After penetrating through the sample solution, the attenuated excitation laser beam was split into two parts by a beam splitter. The nonlinear refraction signal is then measured by a detector with an aperture in front of it, while the nonlinear absorption signal is measured by a detector without an aperture in front of it.

For the measurements of Z-scan and two-photon excited fluorescence emission, 100 fs pulses with wavelengths from 620 to 720 nm and a repetition rate of 1000 Hz were used as the excitation source. The two-photon excited fluorescence signal was dispersed by a 750 mm monochromator combined with suitable filters and detected by a photomultiplier using the standard lock-in amplifier technique.

## 3. RESULTS AND DISCUSSION

Figure 1(a) shows the linear absorption and fluorescence spectra of the perovskite NCs. Here, the band-edge absorption peaks of the perovskite NCs were at 398 nm and 432 nm, respectively. Their fluorescence spectra are centered at 409 and 447 nm, which correspond to non-resonant Stokes shifts of 11 nm and 15 nm. The different Stokes shifts in $CsPbCl_3$ and $CsPb(Cl_{0.53}Br_{0.47})_3$ NCs originate from the existence of different band-edge excitonic fine structures [20]. The TEM images of perovskite NCs are shown in Figs. 1(b) and 1(c), and both of them display a nearly cubic shape. The average edge lengths of $CsPbCl_3$ and $CsPb(Cl_{0.53}Br_{0.47})_3$ NCs are about 9.8 nm and 11.6 nm, which are comparable with the exciton Bohr diameters of the perovskite NCs ($CsPbBr_3$: ~7 nm, $CsPbCl_3$: ~5 nm) [21]. The high-resolution TEM images in the insets of Figs. 1(b) and 1(c) show the crystalline nature of the perovskite NCs. The time-resolved fluorescence decay curves of the NCs are shown in Fig. 1(d). By fitting with an exponential function, we obtained radiative lifetime values of $2.13 \pm 0.08$ ns for $CsPbCl_3$ and $3.99 \pm 0.02$ ns for $CsPb(Cl_{0.53}Br_{0.47})_3$. The lifetime values of the perovskite NCs are about one or two orders of magnitude smaller than those of $MAPbX_3$ ($MA = CH_3NH_3$, X = Cl, Br, I) NCs (~94 ns or 446 ns) [22,23].

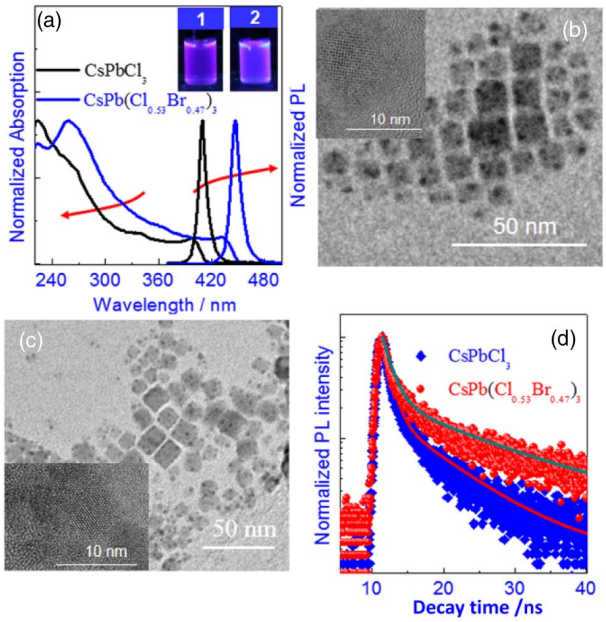


**Fig. 1.** (a) Normalized linear absorption and fluorescence spectra for the perovskite NCs. The insets are the emission images of the NCs in solution: 1 for $CsPbCl_3$ NCs and 2 for $CsPb(Cl_{0.53}Br_{0.47})_3$ NCs. TEM images of (b) $CsPbCl_3$ NCs and (c) $CsPb(Cl_{0.53}Br_{0.47})_3$ NCs. The insets are high-resolution TEM images of the NCs. (d) Fluorescence decay kinetics of the perovskite NCs under excitation at 365 nm.

The value of $\sigma_{lin}$ is an important factor that is used to determine the molar concentration and TPA cross-sections of semiconductor NCs. However, most $\sigma_{lin}$ values of semiconductor NCs have been determined using inductively coupled plasma-atomic emission spectrometry (ICP-AES), which is very challenging due to their size and composition inhomogeneity and the disturbance from the indispensable surface ligands. As a result, the reported TPA cross sections vary by up to 1 order of magnitude among semiconductor NCs, even within the same class [13,15]. Here, we attempt to estimate the $\sigma_{lin}$ values of $CsPbCl_3$ and $CsPb(Cl_{0.53}Br_{0.47})_3$ from the excitation intensity-dependent one-photon induced ground state bleaching (GSB) signals by using fs-TA spectroscopy [14]. TA spectra of NCs in hexane, pumped at 350 nm, are shown in the insets of Figs. 2(a) and 2(c). Both $CsPbCl_3$ and $CsPb(Cl_{0.53}Br_{0.47})_3$ NCs exhibit three distinctive spectral features, including GSB bands centered at 398 nm and 432 nm, respectively. The energy of the GSB agrees well with the lowest-energy excitonic band and thus can be attributed to state-filling-induced beaching. Furthermore, there are two bands of photoinduced absorption (PA) for both $CsPbCl_3$ and $CsPb(Cl_{0.53}Br_{0.47})_3$ NCs. The short-lived PA at the energies just below the band gap mostly likely derives from a band gap renormalization, leading to a momentary increase in the unoccupied states at energies slightly below the ground state band gap [24,25]. As for the PA above the band gap, it likely corresponds to increased scattering from the photorefractive effect of the NCs' suspension. The excitation intensity-dependent fs-TA kinetics for the wavelength of the maximum GSB of $CsPbCl_3$ and $CsPb(Cl_{0.53}Br_{0.47})_3$ NCs was probed [Figs. 2(a) and 2(c)]. After fast Auger recombination within the initial hundreds of picoseconds, the NCs contain only a single exciton in the following time period, which is demonstrated by the parallel decay lines from all the excitation intensities after a long time delay (>0.5 ns). The GSB signal amplitude under different excitation intensities varies according to

$$-A(I/I_0) = -A_{max}[1 - e^{-(I/I_0)\cdot\sigma\cdot I_0}], \quad (1)$$

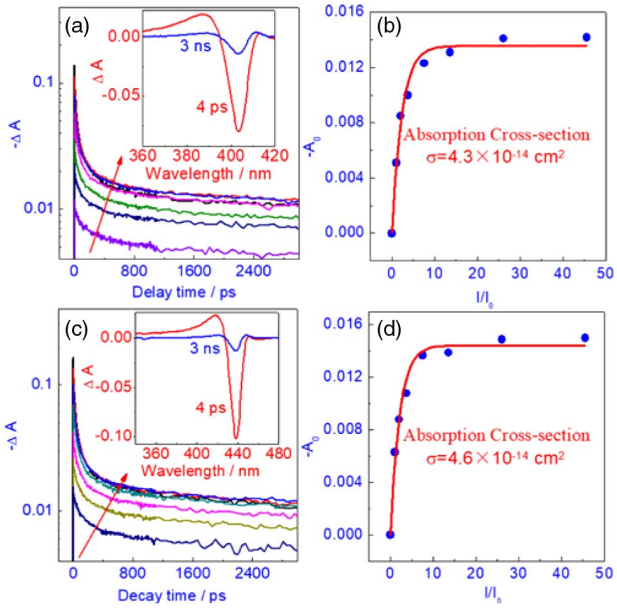


**Fig. 2.** TA kinetics (a) for $CsPbCl_3$ NCs probed at 398 nm and (c) for $CsPb(Cl_{0.53}Br_{0.47})_3$ NCs probed at 432 nm. Initially, the presence of biexcitons and even higher order multi-excitons causes a fast decay (Auger process). At time ≥1 ns, the signals decay exponentially, which corresponds to a single-exciton signal. GSB signal amplitude at a time delay of 1 ns as a function of excitation intensity for (b) $CsPbCl_3$ NCs and (d) $CsPb(Cl_{0.53}Br_{0.47})_3$ NCs.

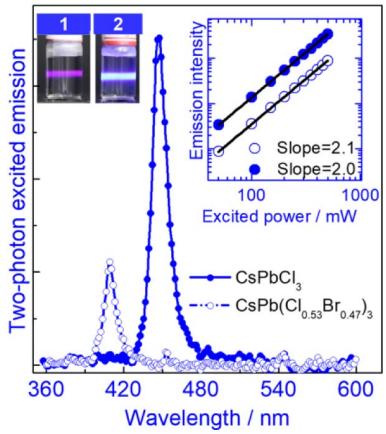


**Fig. 3.** Measured fluorescence intensity as a function of the input laser intensity at 650 nm. The insets are the two-photon excited emission imaging of the NC solution and the best-fitting straight lines on logarithmic scales: 1 for $CsPbCl_3$ NCs and 2 for $CsPb(Cl_{0.53}Br_{0.47})_3$ NCs. The concentration of $CsPb(Cl_{0.53}Br_{0.47})_3$ NCs solution is $1 \times 10^{-6}$ M, while the concentration of $CsPbCl_3$ NCs solution is $2.57 \times 10^{-6}$ M.

where $A(I/I_0)$ denotes the GSB signal amplitude of NCs after a long time delay as a function of excitation intensity, and $I_0$ is the minimum excitation intensity used in the fs-TA experiment [14]. As shown in Figs. 2(b) and 2(c), the excitation intensity-dependent GSB signal amplitude with a delay time of 1 ns could be well fitted with Eq. (1), from which the values of $\sigma_{lin}$ were extracted to be $\sim 4.3 \times 10^{-14}$ $cm^2$ for $CsPbCl_3$ NCs and $\sim 4.6 \times 10^{-14}$ $cm^2$ for $CsPb(Cl_{0.53}Br_{0.47})_3$ NCs. Correspondingly, their molar distinction coefficients were determined to be $1.2 \times 10^7$ and $1.3 \times 10^7$ $L \cdot cm^{-1} \cdot mol^{-1}$ at 350 nm, respectively.

Subsequently, the TPA properties of NCs were investigated. Upon excitation with femtosecond pulses at 650 nm, both the $CsPbCl_3$ and $CsPb(Cl_{0.53}Br_{0.47})_3$ NCs emitted blue fluorescence from hexane solution (inset of Fig. 3, with the excitation light blocked by a low-pass filter). Since linear absorption beyond 450 nm was absent for the studied $CsPbCl_3$ and $CsPb(Cl_{0.53}Br_{0.47})_3$ NCs, the observed fluorescence was thus plausibly attributed to TPA. To verify the TPA mechanism, we measured the fluorescence intensity as a function of the intensities of the input laser pulses. The experimental data are shown in the insets of Fig. 3 on logarithmic scales, in which the data excited at 650 nm can be well fitted by straight lines with slopes of around 2. These results indicated the two-photon excitation features [26]. It is worth noting that the two-photon brightness from the $CsPb(Cl_{0.53}Br_{0.47})_3$ NCs was 2.88 times stronger than that from the $CsPbCl_3$ NCs. Considering 2.57 times higher concentration and 1.90 times lower QY of $CsPbCl_3$ NCs, the stronger two-photon brightness of the $CsPb(Cl_{0.53}Br_{0.47})_3$ NCs should arise from their larger TPA cross sections. The TPA cross sections of NCs were then determined by the open-aperture Z-scan technique.

Figure 4(a) shows the open-aperture Z-scan data for $CsPbCl_3$, $CsPb(Cl_{0.53}Br_{0.47})_3$ NCs and pure hexane at 650 nm. Obviously, the $CsPb(Cl_{0.53}Br_{0.47})_3$ NCs even with very low molar concentration ($\sim 5.95 \times 10^{-6}$ M, 1 M = 1 mol/L) exhibit much stronger signal compared to the pure hexane. Additionally, the experimental data points and the fitting curve show high degrees of correlation. However, even using the same light intensity and solution concentration, the TPA signal of $CsPbCl_3$ NCs is only slightly larger than that of pure hexane. It can be further confirmed that the TPA for $CsPbCl_3$ NCs should be much less than that for $CsPb(Cl_{0.53}Br_{0.47})_3$ NCs. Performing these femtosecond Z-scan experiments at various wavelengths allowed the determination of the TPA spectra of NCs. After the subtraction of the solvent contribution to the measured overall nonlinear absorption, the corresponding TPA spectra are calculated and presented in Fig. 4(b). From

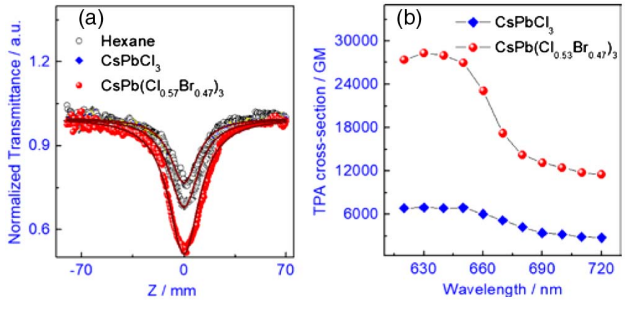


**Fig. 4.** (a) Divided Z-scan results of the OA signal for NCs at a wavelength of 650 nm. The solid lines are the fittings to the data using the Z-scan theory. (b) TPA spectra of NCs between 620 and 720 nm. The concentration of both $CsPbCl_3$ and $CsPb(Cl_{0.53}Br_{0.47})_3$ NCs was $5.95 \times 10^{-6}$ M.

**Table 1. Calculated NLO Parameters of the $CsPbCl_3$ and $CsPb(Cl_{0.53}Br_{0.47})_3$ NCs and Other Materials Reported Elsewhere**

| Samples | $\lambda_{em}$ (nm) | $\sigma_2$ (GM) or $\beta$ (cm/W) | $n_2$ (intrinsic) ($cm^2/W$) | References |
|---|---|---|---|---|
| *p*-Septiphenyl | Violet-blue | 880 GM (0.5 ps, 660 nm) | — | [27] |
| Ladder-type oligo(*p*-phenylene)s | 449 nm | 1046 GM (120 fs, 880 nm) | — | [28] |
| Diphenylamino and 1,2,4-triazole endcapped oligofluorenes | 422 nm | 57 GM (100 fs, 800 nm) | — | [29] |
| Bis(styryl)benzene derivatives | 455 nm | 995 GM (725 nm) | — | [30] |
| ZnS | Violet-blue | 21100 GM (28 ps, 532 nm) or 17200 GM (28 ps, 520 nm) | — | [31] |
| ZnSe/ZnS | 420 nm or 408 nm | 5100 GM or 13900 GM (100 fs, 806 nm) | — | [32] |
| ZnSe | 420 nm or 408 nm | 4900 GM or 12200 GM (100 fs, 806 nm) | — | [32] |
| Truxene-based star-shaped oligofluorenes | 441 nm | 2200 GM (120 fs, 800 nm) | — | [33] |
| 1,4-Bis(carbazolyl)benzene derivatives | 395 nm | 448 GM (100 fs, 720 nm) | — | [34] |
| $CsPbCl_3$ | 456 nm | $1.36 \times 10^{-13}$ cm/W (396 fs, 787 nm) | $5.30 \times 10^{-15}$ (396 fs, 787 nm) | [35] |
| $CsPbBr_3$ | 460 nm | $-1.71 \times 10^{-13}$ cm/W (130 fs, 800 nm) | $-5.18 \times 10^{-13}$ (130 fs, 800 nm) | [36] |
| $CsPb(Cl_{0.53}Br_{0.47})_3$ | 447 nm | 28347 GM or $3.22 \times 10^{-12}$ cm/W (100 fs, 630 nm) | $-1.4 \times 10^{-13}$ (100 fs, 620 nm) | This work |
| $CsPbCl_3$ | 409 nm | 6963 GM or $7.91 \times 10^{-13}$ cm/W (100 fs, 630 nm) | $< -0.46 \times 10^{-13}$ (100 fs, 620 nm) | This work |

Fig. 4(b), for the $CsPbCl_3$ and $CsPb(Cl_{0.53}Br_{0.47})_3$ NCs, their spectral dependence exhibits a general overall decreasing trend with increasing wavelength. It should be attributed to the similar density of the accepting states and similar wavelength dependence of the two electronic transition matrix elements under one- and two-photon excitation [14].

As is expected, compared to $CsPbCl_3$ NCs, much larger values for the TPA cross section were observed in $CsPb(Cl_{0.53}Br_{0.47})_3$ NCs over the entire wavelength range from 620 to 720 nm. The maximum value of the TPA cross section was 28346 GM ($1\ GM = 10^{-50}\ cm^4 \cdot s^{-1} \cdot photon^{-1}$) for $CsPb(Cl_{0.53}Br_{0.47})_3$ NCs and 6963 GM for $CsPbCl_3$ NCs. It is a remarkable fact that the maximum TPA cross section of $CsPb(Cl_{0.53}Br_{0.47})_3$ NCs is 1–2 orders of magnitude higher than the values for most of blue-emitting organic molecules [27–30], and is comparable to those of ZnS, ZnSe, and ZnSe/ZnS NCs [31,32] (Table 1). The two-photon excitation action cross sections ($\sigma_2 \cdot \eta$) per individual NC, the parameters relevant to nonlinear bioimaging, were equal to 480 GM for $CsPbCl_3$ and 3685 GM for $CsPb(Cl_{0.53}Br_{0.47})_3$, which are again among the largest values of blue-emissive NLO materials [33,34] and sufficiently high for the relevant applications (Table 1). Additionally, in order to confirm the validity of our Z-scan measured results, the TPA cross sections of NCs were also determined by the two-photon excited fluorescence method [26] through the comparison of two-photon excited fluorescence intensity of NCs to that of rhodamine 6G. As is expected, the maximum TPA cross sections of the NCs are determined to be 31472 GM for $CsPb(Cl_{0.53}Br_{0.47})_3$ NCs and 7741 GM for $CsPbCl_3$ NCs, which are almost the same as those obtained from the Z-scan method. The consistency between these two methods supports the reliability of the $\sigma_2$ values in this study. In addition, their third-order nonlinear refractive indices ($n_2$) were obtained by fitting the CA Z-scan curves divided by the corresponding OA Z-scan curves (CA/OA) to eliminate the influence of nonlinear absorption [19]. Figure 5(a) shows the CA/OA curves of $CsPbCl_3$ and $CsPb(Cl_{0.53}Br_{0.47})_3$ NCs with a concentration of $5.95 \times 10^{-6}$ M, as well as pure hexane at an intensity of 172 $GW/cm^2$, which were excited at 650 nm. The decreased magnitude of normalized transmittance ($\Delta T$) compared to pure hexane indicates the opposite signs of nonlinear refraction between $CsPb(Cl_{0.53}Br_{0.47})_3$ NCs and hexane, due to a strong positive contribution of the NCs to the hexane solvent. However, the Z-scan signal of the $CsPbCl_3$ NCs solution was almost overlapped with that of the pure hexane solvent, indicating the much smaller nonlinear refraction of $CsPbCl_3$ NCs compared to $CsPb(Cl_{0.53}Br_{0.47})_3$ NCs. By performing these femtosecond Z-scan experiments at various wavelengths again, the wavelength dispersion of nonlinear refraction was obtained, and the maximum third-order nonlinear refractive index of $CsPb(Cl_{0.53}Br_{0.47})_3$ NCs was determined to be $-3.46 \times 10^{-16}$ $cm^2/W$ at 620 nm. For simplicity, we can assume an additive rule for the nonlinear refraction index of the solution

$$n_2(\text{solution}) = g n_2(\text{intrinsic}) + (1-g) n_2(\text{hexane}), \quad \textbf{(2)}$$

where $g$ is the volume fraction of the NCs relative to hexane, $n_2$ (solution) is the total nonlinear refractive index of the NC solution, $n_2$ (intrinsic) is the intrinsic nonlinear refractive index of the NCs, and $n_2$ (solvent) is the nonlinear refractive index of hexane [37]. The maximum value of $n_2$ (intrinsic) for $CsPb(Cl_{0.53}Br_{0.47})_3$ NCs was extracted as $-1.4 \times 10^{-13}$ $cm^2/W$ at 620 nm [Fig. 5(b)]. Meanwhile, considering the resolution of our Z-scan setup, we estimated that the relevant value of $CsPb(Cl_{0.53}Br_{0.47})_3$ NCs should be $< -0.46 \times 10^{-13}$ $cm^2/W$. From the wavelength-dependent nonlinear refractive index curves [Fig. 5(b)], it can be seen that higher nonlinear refraction can be achieved at shorter

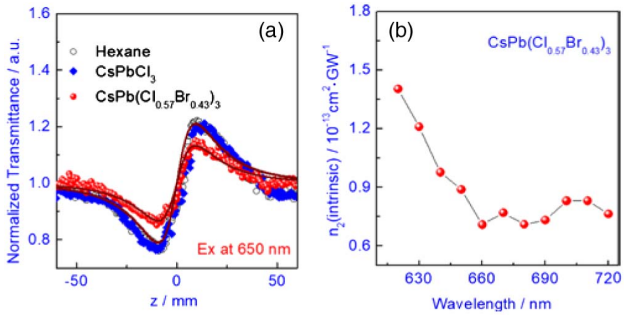


**Fig. 5.** (a) Divided Z-scan results of the CA signal by the OA signal at a wavelength of 650 nm. The solid lines are the fittings to the data using the Z-scan theory. (b) Wavelength-dependent intrinsic nonlinear refractive index of $CsPb(Cl_{0.53}Br_{0.47})_3$ NCs. The concentration of both $CsPbCl_3$ and $CsPb(Cl_{0.53}Br_{0.47})_3$ NCs was $5.95 \times 10^{-6}$ M.

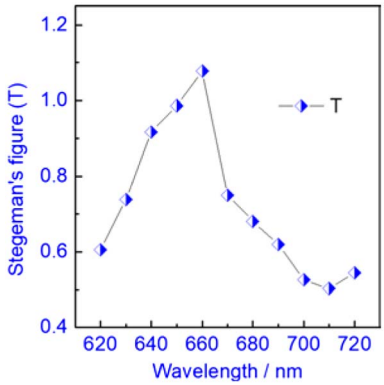


**Fig. 6.** Wavelength-dependent figure of merit ($T$) of $CsPb(Cl_{0.53}Br_{0.47})_3$ NCs.

wavelengths, which should result from the enhanced TPA at shorter wavelengths. According to the analysis by Sheik-Bahae [19], the dominant contribution to the third-order nonlinear refraction in the nonresonant regime arises from the TPA term. On the basis of NLO theory, it can be known that the NLO response of NCs is induced by the distortion of the electron cloud. The differences of NLO properties between $CsPbCl_3$ and $CsPb(Cl_{0.53}Br_{0.47})_3$ NCs indicate that the introduction of $Br^-$ ions has an impact on the formed perovskite crystals. Compared with $CsPbCl_3$ NCs, $CsPb(Cl_{0.53}Br_{0.47})_3$ NCs have higher structural destabilization that will lead to the easier redistribution of the delocalized electrons in $CsPb(Cl_{0.53}Br_{0.47})_3$ [36,38]. Hence, $CsPb(Cl_{0.53}Br_{0.47})_3$ NCs display much stronger nonlinear optical responses. Although the NLO properties of two kinds of blue-emitting perovskite NCs, i.e., $CsPbCl_3$ and $CsPbBr_3$, have been demonstrated in Refs. [35,36], the solution concentrations were not provided and solvent influences on the NLO properties were not discussed. Additionally, there are distinctive differences between our NCs and the reported $CsPbCl_3$ and $CsPbBr_3$ NCs. Thus, direct comparisons between our results and the relevant parameters in Refs. [35,36] are not feasible (Table 1). One thing to be noted is that the wavelength dispersion of TPA and nonlinear refraction of perovskite NCs in our work will facilitate the future potential applications.

In order to evaluate if the $CsPb(Cl_{0.53}Br_{0.47})_3$ NCs can be used in all-optical signal processing devices, such as ultrafast switches, two Stegeman's figures of merit were also calculated [39]. First, the effect of linear absorption must be weaker compared to the effect of nonlinear refraction. This limit can be expressed as $W = n_2 I/\alpha\lambda > 1$, where $I$ is the excitation intensity and $\alpha$ is the linear absorption at the excitation wavelengths. Since linear absorption in $CsPb(Cl_{0.53}Br_{0.47})_3$ NCs is absent at wavelengths of 620–720 nm, the figures of merit $W$ are larger than 1 at all the excitation wavelengths. Therefore, these values satisfy the first Stegeman condition. Second, the effect of TPA must be weaker compared to the nonlinear refraction. This limit can be expressed as $T = \beta\lambda/n_2 < 1$, and values of $T$ of $CsPb(Cl_{0.53}Br_{0.47})_3$ NCs were also calculated, which are smaller than 1 at most of the excitation wavelengths (Fig. 6). Thus, $CsPb(Cl_{0.53}Br_{0.47})_3$ NCs are promising materials for all-optical signal processing devices, considering that two Stegeman figures of merit are satisfied over the wide wavelength range.

## 4. CONCLUSION

In conclusion, we synthesized two colloidal perovskite NCs, i.e., $CsPbCl_3$ and $CsPb(Cl_{0.53}Br_{0.47})_3$, and studied their NLO properties through the Z-scan technique and the two-photon excited fluorescence method. We suggest that both of them are worthy of examination as blue-emitting semiconductor NCs with strong NLO responses. The breaking of the NCs' octahedral symmetry by the introduction of Br anions could be responsible for the larger NLO properties of $CsPb(Cl_{0.53}Br_{0.47})_3$ compared with those of $CsPbCl_3$, which indicates that strong tunability of perovskite NCs can be achieved by subtle variations in composition. Moreover, the stronger TPA and nonlinear refraction of $CsPb(Cl_{0.53}Br_{0.47})_3$ NCs indicate that they should have promising applications in two-photon excited upconverted lasing, multicolor two-photon bioimaging, and all-optical switching.

**Funding.** Shenzhen Basic Research Project of Science and Technology (JCYJ20150324141711631, JCYJ20170302142433007); National Natural Science Foundation of China (NSFC) (11404092, 11404219, 11574130).

†These authors contributed equally to this work.

## REFERENCES

1. T. He, Y. Gao, S. Sreejith, X. Tian, L. Liu, Y. Wang, H. Joshi, S. Z. F. Phua, S. Yao, X. Lin, Y. Zhao, A. C. Grimsdale, and H. Sun, "Biocompatible two-photon absorbing dipyridyldiketopyrrolopyrroles for metal-ion-mediated self-assembly modulation and fluorescence imaging," Adv. Opt. Mater. **4**, 746–755 (2016).
2. T. He, W. Hu, H. Shi, Q. Pan, and X. Lin, "Strong nonlinear optical phosphorescence from water-soluble polymer dots: towards the application of two-photon bioimaging," Dyes Pigm. **123**, 218–221 (2015).
3. J. Li, H. Dong, B. Xu, S. Zhang, Z. Cai, J. Wang, and L. Zhang, "$CsPbBr_3$ perovskite quantum dots: saturable absorption properties and passively Q-switched visible lasers," Photon. Res. **5**, 457–460 (2017).

4. S. Lu, Y. Ge, Z. Sun, Z. Huang, R. Cao, C. Zhao, S. Wen, D. J. Li, and H. Zhang, "Ultrafast nonlinear absorption and nonlinear refraction in few-layer oxidized black phosphorus," Photon. Res. **4**, 286–292 (2016).
5. T. He, S. Yao, J. Zhang, Y. Li, X. Li, J. Hu, R. Chen, and X. Lin, "Strong multiphoton absorption properties of one styrylpyridinium salt in a highly polar solvent," Opt. Express **24**, 11091–11102 (2016).
6. T. He, J. Li, C. Ren, S. Xiao, Y. Li, R. Chen, and X. Lin, "Strong two-photon absorption of Mn-doped $CsPbCl_3$ perovskite nanocrystals," Appl. Phys. Lett. **111**, 211105 (2017).
7. A. K. Mandal, S. Sreejith, T. He, S. K. Maji, X. Wang, S. L. Ong, J. Joseph, H. Sun, and Y. Zhao, "Three-photon-excited luminescence from unsymmetrical cyanostilbene aggregates: morphology tuning and targeted bioimaging," ACS Nano **9**, 4796–4805 (2015).
8. Y. Wang, V. D. Ta, Y. Gao, T. C. He, R. Chen, E. Mutlugun, H. V. Demir, and H. D. Sun, "Stimulated emission and lasing from CdSe/CdS/ZnS core-multi-shell quantum dots by simultaneous three-photon absorption," Adv. Mater. **26**, 2954–2961 (2014).
9. W. Hu, T. He, R. Jiang, J. Yin, L. Li, X. Lu, H. Zhao, L. Zhang, L. Huang, H. Sun, W. Huang, and Q. Fan, "Inner salt-shaped small molecular photosensitizer with extremely enhanced two-photon absorption for mitochondrial-targeted photodynamic therapy," Chem. Commun. **53**, 1680–1683 (2017).
10. T. He, P. C. Too, R. Chen, S. Chiba, and H. Sun, "Concise synthesis and two-photon-excited deep-blue emission of 1,8-diazapyrenes," Chem. Asian J. **7**, 2090–2095 (2012).
11. W. Hu, M. Xie, H. Zhao, Y. Tang, S. Yao, T. He, C. Ye, Q. Wang, X. Lu, W. Huang, and Q. Fan, "Nitric oxide activatable photosensitizer accompanying extremely elevated two-photon absorption for efficient fluorescence imaging and photodynamic therapy," Chem. Sci. **9**, 999–1005 (2018).
12. K. Wei, Z. Xu, R. Chen, X. Zheng, X. Cheng, and T. Jiang, "Temperature-dependent excitonic photoluminescence excited by two-photon absorption in perovskite $CsPbBr_3$ quantum dots," Opt. Lett. **41**, 3821–3824 (2016).
13. Y. Wang, X. Li, X. Zhao, L. Xiao, H. Zeng, and H. Sun, "Nonlinear absorption and low-threshold multiphoton pumped stimulated emission from all-inorganic perovskite nanocrystals," Nano Lett. **16**, 448–453 (2016).
14. J. Chen, K. Žídek, P. Chábera, D. Liu, P. Cheng, L. Nuuttila, M. J. Al-Marri, H. Lehtivuori, M. E. Messing, K. Han, K. Zheng, and T. Pullerits, "Size- and wavelength-dependent two-photon absorption cross-section of $CsPbBr_3$ perovskite quantum dots," J. Phys. Chem. Lett. **8**, 2316–2321 (2017).
15. Y. Xu, Q. Chen, C. Zhang, R. Wang, H. Wu, X. Zhang, G. Xing, W. W. Yu, X. Wang, Y. Zhang, and M. Xiao, "Two-photon-pumped perovskite semiconductor nanocrystal lasers," J. Am. Chem. Soc. **138**, 3761–3768 (2016).
16. X. Wang, H. Zhou, S. Yuan, W. Zheng, Y. Jiang, X. Zhuang, H. Liu, Q. Zhang, X. Zhu, X. Wang, and A. Pan, "Cesium lead halide perovskite triangular nanorods as high-gain medium and effective cavities for multiphoton-pumped lasing," Nano Res. **10**, 3385–3395 (2017).
17. W. Chen, S. Bhaumik, S. A. Veldhuis, G. Xing, Q. Xu, M. Gratzel, S. Mhaisalkar, N. Mathews, and T. C. Sum, "Giant five-photon absorption from multidimensional core-shell halide perovskite colloidal nanocrystals," Nat. Commun. **8**, 15198 (2017).
18. J. Song, J. Li, X. Li, L. Xu, Y. Dong, and H. Zeng, "Quantum dot light-emitting diodes based on inorganic perovskite cesium lead halides ($CsPbX_3$)," Adv. Mater. **27**, 7162–7167 (2015).
19. M. Sheik-Bahae, A. A. Said, T.-H. Wei, D. J. Hagan, and E. W. Van Stryland, "Sensitive measurement of optical nonlinearities using a single beam," IEEE J. Quantum Electron. **26**, 760–769 (1990).
20. M. C. Brennan, J. Zinna, and M. Kuno, "Existence of a size-dependent Stokes shift in $CsPbBr_3$ perovskite nanocrystals," ACS Energy Lett. **2**, 1487–1488 (2017).
21. L. Protesescu, S. Yakunin, M. I. Bodnarchuk, F. Krieg, R. Caputo, C. H. Hendon, R. X. Yang, A. Walsh, and M. V. Kovalenko, "Nanocrystals of cesium lead halide perovskites ($CsPbX_3$, X = Cl, Br, and I): novel optoelectronic materials showing bright emission with wide color gamut," Nano Lett. **15**, 3692–3696 (2015).
22. C. Wehrenfennig, M. Liu, H. J. Snaith, M. B. Johnston, and L. M. Herz, "Homogeneous emission line broadening in the organo lead halide perovskite $CH_3NH_3PbI_{3-x}Cl_x$," J. Phys. Chem. Lett. **5**, 1300–1306 (2014).
23. M. Zhang, H. Yu, M. Lyu, Q. Wang, J. Yun, and L. Wang, "Composition-dependent photoluminescence intensity and prolonged recombination lifetime of perovskite $CH_3NH_3PbBr_{3-x}Cl_x$ films," Chem. Commun. **50**, 11727–11730 (2014).
24. J. Butkus, P. Vashishtha, K. Chen, J. K. Gallaher, S. K. K. Prasad, D. Z. Metin, G. Laufersky, N. Gaston, J. E. Halpert, and J. M. Hodgkiss, "The evolution of quantum confinement in $CsPbBr_3$ perovskite nanocrystals," Chem. Mater. **29**, 3644–3652 (2017).
25. N. S. Makarov, S. Guo, O. Isaienko, W. Liu, I. Robel, and V. I. Klimov, "Spectral and dynamical properties of single excitons, biexcitons, and trions in cesium-lead-halide perovskite quantum dots," Nano Lett. **16**, 2349–2362 (2016).
26. G. S. He, L. S. Tan, Q. Zheng, and P. N. Prasad, "Multiphoton absorbing materials: molecular designs, characterizations, and applications," Chem. Rev. **108**, 1245–1330 (2008).
27. G. S. He, G. C. Xu, P. N. Prasad, B. A. Reinhardt, J. C. Bhatt, and A. G. Dillard, "Two-photon absorption and optical-limiting properties of novel organic compounds," Opt. Lett. **20**, 435–437 (1995).
28. H. Fan, L. Guo, K. Li, M. Wong, and K. W. Cheah, "Exceptionally strong multiphoton-excited blue photoluminescence and lasing from ladder-type oligo(*p*-phenylene)s," J. Am. Chem. Soc. **134**, 7297–7300 (2012).
29. P. L. Wu, X. Feng, H. L. Tam, M. S. Wong, and K. W. Cheah, "Efficient three-photon excited deep blue photoluminescence and lasing of diphenylamino and 1,2,4-triazole endcapped oligofluorenes," J. Am. Chem. Soc. **131**, 886–887 (2009).
30. M. Albota, D. Beljonne, J. Brédas, J. E. Ehrlich, J. Fu, A. A. Heikal, S. E. Hess, T. Kogej, M. D. Levin, S. R. Marder, D. McCord-Maughon, J. W. Perry, H. Röckel, M. Rumi, G. Subramaniam, W. W. Webb, X.-L. Wu, and C. Xu, "Design of organic molecules with large two-photon absorption cross sections," Science **281**, 1653–1656 (1998).
31. V. V. Nikesh, A. Dharmadhikari, H. Ono, S. Nozaki, G. R. Kumar, and S. Mahamuni, "Optical nonlinearity of monodispersed, capped ZnS quantum particles," Appl. Phys. Lett. **84**, 4602–4604 (2004).
32. A. D. Lad, P. P. Kiran, D. More, G. R. Kumar, and S. Mahamuni, "Two-photon absorption in ZnSe and ZnSe/ZnS core/shell quantum structures," Appl. Phys. Lett. **92**, 043126 (2008).
33. B. Guzelturk, A. L. Kanibolotsky, C. Orofino-Pena, N. Laurand, M. D. Dawson, P. J. Skabara, and H. V. Demir, "Ultralow-threshold up-converted lasing in oligofluorenes with tailored strong nonlinear absorption," J. Mater. Chem. C **3**, 12018–12025 (2015).
34. B. Zhao, X. Jia, J. Liu, X. Ma, H. Zhang, X. Wang, and T. Wang, "Synthesis and characterization of novel 1,4-bis(carbazolyl)benzene derivatives with blue-violet two-photon-excited fluorescence," Ind. Eng. Chem. Res. **55**, 1801–1807 (2016).
35. S. Liu, G. Chen, Y. Huang, S. Lin, Y. Zhang, M. He, W. Xiang, and X. Liang, "Tunable fluorescence and optical nonlinearities of all inorganic colloidal cesium lead halide perovskite nanocrystals," J. Alloys Compd. **724**, 889–896 (2017).
36. W.-G. Lu, C. Chen, D. Han, L. Yao, J. Han, H. Zhong, and Y. Wang, "Nonlinear optical properties of colloidal $CH_3NH_3PbBr_3$ and $CsPbBr_3$ quantum dots: a comparison study using Z-scan technique," Adv. Opt. Mater. **4**, 1732–1737 (2016).
37. G. S. He, J. Zhu, A. Baev, M. Samoć, D. L. Frattarelli, N. Watanabe, A. Facchetti, H. Ågren, T. J. Marks, and P. N. Prasad, "Twisted $\pi$-system chromophores for all-optical switching," J. Am. Chem. Soc. **133**, 6675–6680 (2011).
38. R. Zhang, J. Fan, X. Zhang, H. Yu, H. Zhang, Y. Mai, T. Xu, J. Wang, and H. J. Snaith, "Nonlinear optical response of organic-inorganic halide perovskites," ACS Photon. **3**, 371–377 (2016).
39. G. I. Stegeman, "Material figures of merit and implications to all-optical waveguide switching," Proc. SPIE **1852**, 75–89 (1993).